Proceedings of the ASME 2018 Turbomachinery Technical Conference & Exposition
ASME 2018 Turbo Expo
June 11-15, 2018, Lillestrøm, Oslo, Norway

GT2018-76797

EFFECTS OF ASYMMETRY ON THERMOACOUSTIC MODES IN ANNULAR COMBUSTORS: A HIGHER-ORDER PERTURBATION STUDY

Georg A. Mensah,*[1] Luca Magri,[2] Alessandro Orchini,[1] and Jonas P. Moeck[1,3]

[1]Institut für Strömungsmechanik und Technische Akustik
Technische Universität Berlin
Berlin, Germany
E-mail: georg.a.mensah@tu-berlin.de

[2]Engineering Department
University of Cambridge
Cambridge, UK

[3]Department of Energy and Process Engineering
Norwegian University of Science and Technology
Trondheim, Norway

ABSTRACT

Gas-turbine combustion chambers typically consist of nominally identical sectors arranged in a rotationally symmetric pattern. However, in practice the geometry is not perfectly symmetric. This may be due to design decisions, such as placing dampers in an azimuthally non-uniform fashion, or to uncertainties in the design parameters, which break the rotational symmetry of the combustion chamber. The question is whether these deviations from symmetry have impact to the thermoacoustic-stability calculation. The paper addresses this question by proposing a fast adjoint-based perturbation method. This method can be integrated into numerical frameworks that are industrial standard such as lumped-network models, Helmholtz- and linearized Euler-equations. The thermoacoustic stability of asymmetric combustion chambers is investigated by perturbing rotationally symmetric combustor models. The approach proposed in this paper is applied to a realistic three-dimensional combustion chamber model with an experimentally measured flame transfer function, which is solved with a Helmholtz solver. Results for modes of zeroth, first, and second azimuthal mode order are presented and compared to exact solutions of the problem. A focus of the discussion is set on the loss of mode-degeneracy due to symmetry breaking and the capability of the perturbation theory to accurately predict it. In particular, an "inclination rule" that explains the behavior of degenerate eigenvalues at first order is proven.

NOMENCLATURE

Roman

$\boldsymbol{B}$	FEM discretization matrix for the BCs
c_0	Speed of sound
i	Imaginary unit
$\boldsymbol{K}$	FEM discretization matrix for the second derivative
$\mathcal{L}$	Linear operator
$\boldsymbol{M}$	FEM discretization matrix for identity
$\widehat{p}$	Fourier transform of acoustic pressure
$\boldsymbol{Q}$	FEM discretization of the heat release operator
q_0	Mean heat release rate
$\boldsymbol{S}_i$	state-space matrices
$\boldsymbol{s}$	system state
t	Time
u_0	Mean velocity at which FTF was calculated

*Address all correspondence to this author.

$\boldsymbol{X}, \boldsymbol{Y}$	Matrices of the auxiliary eigenvalue problem
Z	Impedance
$\boldsymbol{z}$	Eigenvector of the auxiliary eigenvalue problem

Greek

γ	Ratio of specific heats
ε	Design parameter
$\boldsymbol{\varepsilon}$	Vector of design parameters
$\Delta\varepsilon_n$	Perturbation of the nth design parameter with respect to the baseline
μ	Scaling perturbation parameter
ρ_0	Density
ω	Complex eigenfrequency

INTRODUCTION

Thermoacoustic instabilities pose a major threat to modern gas turbines. They may cause severe damage to the machines, limit their lifetime, lead to an increase of pollutant emissions, and trigger strong noise exposure [1,2]. The availability of mathematical and computational design tools to the developers of new gas turbines is, thus, essential [3]. Although Large-Eddy Simulations (LES) resolve the relevant physics down to small scales, they are inefficient when the effects of a large set of parameters on the thermoacoustic stability need to be investigated. This is because of the large computational cost of LES. Early-stage gas turbine development, thus, often resorts to linear frequency-domain based approaches, such as low-order network models [4] and solutions of the thermoacoustic Helmholtz equation [5].

Frequency-based models of thermoacoustic systems typically result in eigenvalue problems that are nonlinear with respect to their eigenvalue – the complex eigenfrequency ω

$$\mathcal{L}(\omega, \boldsymbol{\varepsilon})\widehat{p} = 0, \tag{1}$$

where $\mathcal{L}$ denotes a linear operator, $\widehat{p}$ the eigenvector, ω the corresponding eigenvalue that may appear under nonlinear terms, and $\boldsymbol{\varepsilon}$ a vector of design parameters. The dependency of the solutions on the design parameters is, however, not explicit. Hence, several solutions of the eigenvalue problem have to be computed to infer explicit relations for $\omega = \omega(\boldsymbol{\varepsilon})$ and $\widehat{p} = \widehat{p}(\boldsymbol{\varepsilon})$. This is generally a laborious and non-efficient task.

Thermoacoustic problems depend on many parameters, but only a handful of modes are of interest. Adjoint perturbation theory enables the calculation of explicit relations between the solutions of the perturbed eigenvalue problem and the many design parameters. The calculation by adjoint methods is computationally cheap and accurate. For these reasons, adjoint methods have been recently applied to thermoacoustic stability analysis [6,7].

Adjoint methods were subsequently applied to uncertainty quantification of thermoacoustic stability with wave approaches in annular combustors [8] and with a Helmholtz solver for a swirled turbulent longitudinal combustor [9]. To avoid the Monte-Carlo sampling, the probability that a dump combustor becomes unstable was calculated by high-order adjoint perturbation methods, which enabled for the calculation of the stability boundary with an algebraic expression [10].

Focusing on annular combustors, [11] computed the thermoacoustic modes with a Helmholtz solver by applying Bloch-wave theory to only one sector. By using adjoint methods, they calculated the sensitivity of the degenerate eigenvalue to asymmetries in the flame transfer function due, for example, to variations in the mean flow. The gradient information was then embedded in an optimization algorithm to maximize the damping by optimal placement and tuning of acoustic dampers in an annular combustor [12].

The aim of this paper is to apply high-order adjoint perturbation theory to practical annular combustors. Such combustors have discrete rotational symmetry, which causes many of the eigenmodes to be degenerate. In other words, two eigenmodes may be associated with the same eigenvalue, but different eigenvectors. This observation has significant consequences on the correct application of adjoint perturbation theory to symmetry-breaking perturbations. Symmetry-breaking with regard to annular combustion chambers has been discussed in recent experimental and analytical studies, e.g. [13,14,15,16].

The paper is organized as follows. First, the theory of both frequency-domain-based thermoacoustic stability assessment and adjoint perturbation theory is presented. Second, the theory is applied to the well-studied annular combustor model, namely the MICCA combustor. Third, a short mathematical proof explaining the phase of the first-order eigenvalue shifts in the complex plane is given. The paper concludes with remarks on why the findings are useful for practical gas turbine design.

THEORY

Thermoacoustic Helmholtz Equation

By linearizing the equations of conservation of mass, momentum and entropy for a fluid at rest, the thermoacoustic Helmholtz equation can be obtained after appropriate combinations of the equations [5]

$$\nabla\cdot(c_0^2\nabla\widehat{p}) + \omega^2\widehat{p} = -(\gamma-1)\mathrm{i}\omega\widehat{q}. \tag{2}$$

Here, c_0 denotes the speed of sound, γ is the ratio of specific heats, and $\widehat{p}$ and $\widehat{q}$ are the the Fourier transforms of the pressure and heat-release fluctuations, respectively.

The $(\cdot)(t) \mapsto \widehat{(\cdot)}\exp(\mathrm{i}\omega t)$ convention is used to define the Fourier transform. The fluctuating part of the heat release rate is related to velocity fluctuations at a reference point by a flame

transfer function (FTF)

$$\widehat{q} = \frac{q_0}{u_0}\,\mathrm{FTF}(\omega)\vec{u}_{ref}\cdot\vec{n}_{\mathrm{ref}}. \tag{3}$$

In this relation, q_0 denotes the mean heat-release rate, u_0 is the mean velocity at the reference position, $\vec{u}_{ref}$ is the velocity fluctuation at a reference position, and $\vec{n}_{\mathrm{ref}}$ is a unit vector, which represents a reference direction. By relating the velocity fluctuation to the pressure gradient via the linearized momentum balance, the following eigenvalue problem is obtained

$$\nabla\cdot(c_0^2\nabla\widehat{p}) + \omega^2\widehat{p} - \frac{\gamma-1}{\rho_0}\,\mathrm{FTF}(\omega)\nabla\widehat{p}_{\mathrm{ref}}\cdot\vec{n}_{\mathrm{ref}} = 0, \tag{4}$$

where ρ_0 denotes the mean gas density at the reference position. The boundary conditions are provided by

$$\widehat{p} - \frac{\mathrm{i}c_0 Z}{\omega}\nabla\widehat{p}\cdot\vec{n} = 0, \tag{5}$$

where Z denotes the impedance and $\vec{n}$ is the outward pointing unit normal vector.

For the current study the eigenvalue problem is discretized by a finite element method, which utilizes tetrahedral linear Lagrange elements. This leads to the following disrcretized form of the thermoacoustic Helmholtz equation

$$\Big(\boldsymbol{K} + \omega\boldsymbol{B} + \omega^2\boldsymbol{M} + \boldsymbol{Q}(\omega)\Big)\boldsymbol{p} = 0 \tag{6}$$

where $\boldsymbol{p}$ is the discretized pressure fluctuation amplitude, $\boldsymbol{K}$ denotes the discretization matrix for $\nabla\cdot c_0^2\nabla$-operation (also known as the stiffness matrix), $\boldsymbol{M}$ refers to the discretization of the identity operation (also known as the mass matrix), $\boldsymbol{B}$ is the discretization matrix arising from the boundary conditions, and $\boldsymbol{Q}$ denotes the discretized heat release operator. [5] contains more details on finite element discretizations of the thermoacoustic Helmholtz equation.

High order adjoint perturbation theory is an incremental procedure and, thus, requires accurate solutions of the baseline solution to mitigate the error propagation through the different orders. Therefore, the nonlinear eigenvalue problem is solved using a Newton-type iteration, known as the generalized Rayleigh quotient iteration [17, 18], which is generally faster than the fixed-point iteration proposed in [5]. For the system solved in this study, the Newton-type method converges to machine-precise solutions within 3 up to 7 iterations. It is also adjoint-based and therefore poses the same mathematical requirements to the model as the adjoint perturbation theory. This also makes it easy to be integrated in a software framework that is already designed to perform adjoint perturbation theory such as PyHoltz[1] – the open-source Helmholtz solver used for this study.

Adjoint perturbation theory

The aim of adjoint perturbation theory is to find asymptotic approximations for the dependence of the eigenvalues and eigenfunctions on the parameters of the eigenvalue problem. This mathematical tool is successfully deployed in the field of quantum mechanics to find solutions to the Schrödinger equation. Because the Schrödinger equation has some mathematical similarities to the Helmholtz equation, quantum mechanics techniques can be useful for the study of thermoacoustic instabilities (e.g., [6,11]). The main advantage of adjoint perturbation theory is that good approximations of the actual solutions are found at very low computational costs. This section summarizes the main concepts of the theory.

The discussion starts with a single-parameter third-order theory, which can be turned into a multi-parameter theory by means of a global scaling parameter. Starting from a known solution of the eigenvalue problem of interest

$$\mathcal{L}(\omega_0;\varepsilon_0)\widehat{p}_0 = 0, \tag{7}$$

it is assumed that the change of the eigenmodes due to a change of the parameter ε_0 by a small perturbation $\Delta\varepsilon$ can be described by asymptotic power series

$$\omega(\varepsilon) = \omega_0 + \omega_1(\Delta\varepsilon) + \omega_2(\Delta\varepsilon)^2 + \omega_3(\Delta\varepsilon)^3 + O((\Delta\varepsilon)^4) \tag{8a}$$
$$\widehat{p}(\varepsilon) = \widehat{p}_0 + \widehat{p}_1(\Delta\varepsilon) + \widehat{p}_2(\Delta\varepsilon)^2 + \widehat{p}_3(\Delta\varepsilon)^3 + O((\Delta\varepsilon)^4). \tag{8b}$$

Note, that this assumption implies that the solution is analytic in ε. To find the coefficients appearing in these power series, the ansätze (8) have to be substituted into the eigenvalue problem (1). Thence, the linear operator itself is to be expanded into bivariate Taylor series in ω and ε, and the result must be sorted by powers of $\Delta\varepsilon$. For each order k, this procedure yields an equation of the form

$$\mathcal{L}_{0,0}\widehat{p}_k = -r_k - \omega_k\mathcal{L}_{1,0}\widehat{p}_0, \tag{9}$$

where

$$\mathcal{L}_{m,n} \equiv \frac{1}{m!n!}\,\frac{\partial^{m+n}\mathcal{L}}{\partial\omega^m\partial\varepsilon^n}\bigg|_{\substack{\omega=\omega_0\\ \varepsilon=\varepsilon_0}} \tag{10}$$

[1] http://fd.tu-berlin.de/forschung/projekte/thermoakustik/pyholtz/

For the first three orders the r_k are explicitly given by

$$r_1 \equiv \mathcal{L}_{0,1}\widehat{p}_0 \tag{11a}$$

$$r_2 \equiv \mathcal{L}_{0,1}\widehat{p}_1 + \mathcal{L}_{0,2}\widehat{p}_0 + \omega_1\left(\mathcal{L}_{1,0}\widehat{p}_1 + \mathcal{L}_{1,1}\widehat{p}_0\right) + \omega_1^2\mathcal{L}_{2,0}\widehat{p}_0 \tag{11b}$$

$$\begin{aligned} r_3 \equiv{}& \mathcal{L}_{0,1}\widehat{p}_2 + \mathcal{L}_{0,2}\widehat{p}_1 + \mathcal{L}_{0,3}\widehat{p}_0 + \omega_1\left(\mathcal{L}_{1,0}\widehat{p}_2 + \mathcal{L}_{1,1}\widehat{p}_1 + \mathcal{L}_{1,2}\widehat{p}_0\right) \\ &+ \omega_1^2\left(\mathcal{L}_{2,0}\widehat{p}_1 + \mathcal{L}_{2,1}\widehat{p}_0\right) + \omega_2\left(\mathcal{L}_{1,0}\widehat{p}_1 + \mathcal{L}_{1,1}\widehat{p}_0\right) \\ &+ 2\omega_1\omega_2\mathcal{L}_{2,0}\widehat{p}_0 + \omega_1^3\mathcal{L}_{3,0}\widehat{p}_0. \end{aligned} \tag{11c}$$

By definition, $\mathcal{L}_{0,0}$ is not invertible because it is evaluated at the eigenvalue ω_0. Therefore, for the linear system (9) to have solutions, solvability conditions have to be fulfilled at each order

$$\left\langle \widehat{p}_0^{\dagger} \middle| -r_k - \omega_k\mathcal{L}_{1,0}\widehat{p}_0 \right\rangle = 0, \tag{12}$$

where $\widehat{p}_0^{\dagger}$ denotes the adjoint solution of the eigenvalue problem (7) and $\langle\cdot|\cdot\rangle$ is an inner product. This condition is also known as the Fredholm alternative.

If the problem is not degenerate, i.e., the eigenvalue ω_0 has algebraic multiplicity 1, Eq. (12) can be readily solved for ω_k. Then, the result can be substituted back into (9) in order to obtain the eigenfunction correction, $\widehat{p}_k$. Instead, if the system is degenerate with multiplicity $D > 1$ (D is an integer) and the algebraic and geometric multiplicities coincide, D solvability conditions have to be fulfilled simultaneously. This gives rise to an auxiliary algebraic eigenvalue problem

$$\boldsymbol{X}_k\boldsymbol{z} - \omega_k\boldsymbol{Y}\boldsymbol{z} = \boldsymbol{0}, \tag{13}$$

where $\boldsymbol{X}_k$ and $\boldsymbol{Y}$ are matrices whose entries are given by the following scalar products

$$[\boldsymbol{X}_k]_{i,j} \equiv \left\langle \widehat{p}_{0,j}^{\dagger} \middle| -r_{k,i} \right\rangle \quad \text{and} \quad [\boldsymbol{Y}]_{i,j} \equiv \left\langle \widehat{p}_{0,j}^{\dagger} \middle| \mathcal{L}_{1,0}\widehat{p}_{0,i} \right\rangle. \tag{14}$$

It can be shown that the bases for the direct and the adjoint eigenspaces – $\mathrm{span}(\widehat{p}_{0,1}, \ldots, \widehat{p}_{0,D})$ and $\mathrm{span}\left(\widehat{p}_{0,1}^{\dagger}, \ldots, \widehat{p}_{0,D}^{\dagger}\right)$ respectively – can be chosen such that $\boldsymbol{Y}$ becomes the identity matrix $\boldsymbol{I}$, see e.g. [18].

If the auxiliary problem is degenerate at kth order, no split of the degenerate eigenspace is detected by the asymptotic theory and the computation involves an auxiliary eigenvalue problem at the next order. Otherwise, the degenerate eigenspace unfolds into subspaces corresponding to different eigenvalues; and the eigendirections of the subspaces are obtained from the eigenvectors $\boldsymbol{z}$ of the first non-degenerate eigenvalue problem.

Mode degeneracy is a relevant problem for annular and can-annular combustors because it is induced by their discrete rotational geometry. The multiplicity of the degeneracy induced by this symmetry is usually $D = 2$.

Up until now the perturbation theory has accounted for one parameter only. However, several parameters are relevant in practical combustor design. By introducing a scaling parameter, multiple parameters can be tuned at once. For example, if there are two design parameters ε_1 and ε_2 such that the eigenvalue problem reads

$$\mathcal{L}(\omega, \varepsilon_1, \varepsilon_2)\widehat{p} = 0, \tag{15}$$

and the change from the parameter tuple $(\varepsilon_{1,0}, \varepsilon_{2,0})$ to the tuple $(\varepsilon_{1,0} + \Delta\varepsilon_1, \varepsilon_{2,0} + \Delta\varepsilon_2)$ has to be computed, then the problem can be rephrased as

$$\left[\mathcal{L}(\omega, \varepsilon_{1,0}, \varepsilon_{2,0})(1-\mu) + \mathcal{L}(\omega, \varepsilon_{1,0} + \Delta\varepsilon_1, \varepsilon_{2,0} + \Delta\varepsilon_2)\mu\right]\widehat{p} = 0. \tag{16}$$

The parameter μ serves as a scaling parameter. For $\mu = 0$ the base-line problem is obtained, while the equation amounts to the fully perturbed problem when μ is set to 1. Hence, the parameter μ can be taken as a single perturbation parameter to spur the asymptotic analysis described above [19]. Alternatively, it would be possible to derive a fully multi-parameter perturbation theory – see e.g. [12] for a first-order multi-parameter theory with application to thermoacoustics.

APPLICATION

The MICCA Annular Combustor

The theory described in the previous section is applied to a laboratory-scale annular combustor configuration, which was designed and built at Laboratoire EM2C, CentraleSupelec (formerly Ecole Centrale Paris) and is referred to as MICCA [20]. Since its introduction it has been the topic of various experimental and numerical studies, e.g. [21, 22, 23, 24]. The geometry features 16 burners and is depicted in Fig. 1.

The combustor has been investigated in many recent studies, both experimentally and numerically. The geometry is discretized using a mesh featuring 14032 points, which form 59840 tetrahedra. Special care was taken to guarantee that the mesh-structure still features the discrete rotational symmetry. Unlike the real geometry, the mesh is not modeling the pressure transducer holes in the plenum. The mesh is shown in Fig. 2 , together with the speed-of-sound field. The latter was set to be identical to the one presented in [23]. Also, the boundary conditions were chosen to be the same as the latter study: a 41 mm end correction was added to the the combustion chamber length, so that a pressure node can be set at the outlet and all other boundaries were

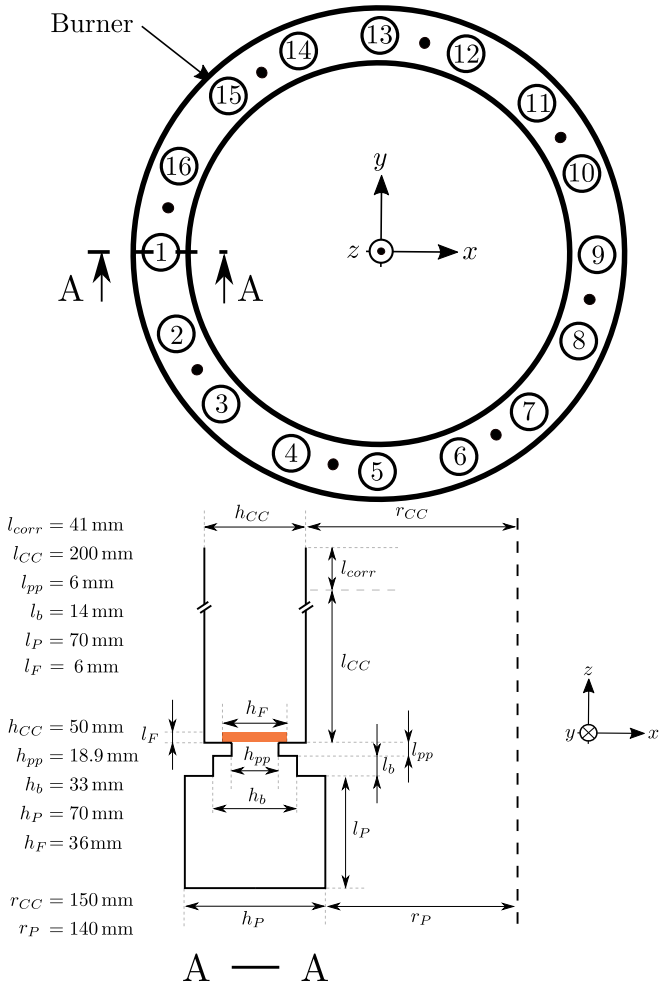

FIGURE 1. Annular combustor geometry used for the present study. The combustor is referred to as MICCA [20]. The domain of heat release is highlighted in orange and is defined as in [23].

specified to feature pressure anti-nodes. The flame transfer function data are also taken from the measured data given in [23]. However, the FTF incorporation into the model is different, due to the special requirements imposed by the adjoint analysis. This will be discussed in the next chapter.

Flame Transfer Function

For the perturbation theory to work, all coefficients should be differentiable with respect to the eigenfrequency ω, which generally is complex-valued. However, the FTF data are measured experimentally only for purely real eigenfrequencies, i.e. with zero growth rate. Hence, an appropriate modeling technique is needed, which reproduces the discrete data samples to a satisfying degree and is analytic. Analyticity is a property required to extrapolate the data into the complex plane in

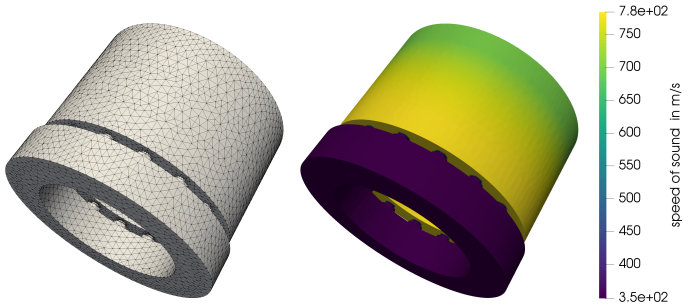

FIGURE 2. Discretization mesh used in this study (left) and mean speed of sound c_0 (right). The color scale ranges from 348 m/s (purple) to 784 m/s (yellow).

a unique and smooth way. For the present study the flame dynamics in the complex plane is modeled by a state-space model. More precisely, measurement data from [23] (operating point B) have been used to fit a linear, six-dimensional state space model, shown in Fig. 3.

The state-space model is described by the following system of differential equations:

$$\frac{\mathrm{d}}{\mathrm{d}t}\boldsymbol{s} = \boldsymbol{S}_1\boldsymbol{s} + \boldsymbol{S}_2 u \tag{17}$$

$$q = \boldsymbol{S}_3\boldsymbol{s} + \boldsymbol{S}_4 u \tag{18}$$

Following the terminology of state space models, u and q denote the input and output to the system, i.e., the reference velocity and corresponding fluctuation of the heat release rate, respectively. Moreover, $\boldsymbol{s}$ is the state vector of the system, $\boldsymbol{S}_1$ the system matrix, $\boldsymbol{S}_2$ the input matrix, $\boldsymbol{S}_3$ the output matrix, and $\boldsymbol{S}_4$ the feedthrough matrix.

In the complex frequency space, the explicit dependence of the heat release rate q on the velocity fluctuations at the reference point, u, is expressed by

$$\widehat{q} = \underbrace{\left(\boldsymbol{S}_3\left(\mathrm{i}\omega\boldsymbol{I} - \boldsymbol{S}_1\right)^{-1}\boldsymbol{S}_2 + \boldsymbol{S}_4\right)}_{\text{FTF}}\widehat{u}. \tag{19}$$

The matrices $\boldsymbol{S}_i$ have been computed with the identification algorithm described in [25, 26]. Importantly, the derivatives of (19) with respect to the eigenfrequency, which are needed in the adjoint-based analysis, can be expressed in closed form and be efficiently and accurately evaluated when the transfer function is expressed in state space form. In particular, by introducing the Kronecker delta $\delta_{i,j}$ we can write

$$\frac{\partial^k}{\partial\omega^k}\mathrm{FTF}(\omega) = (-\mathrm{i})^k k!\boldsymbol{S}_3\left(\mathrm{i}\omega I - \boldsymbol{S}_1\right)^{-(k+1)}\boldsymbol{S}_2 + \boldsymbol{S}_4\delta_{k,0} \tag{20}$$

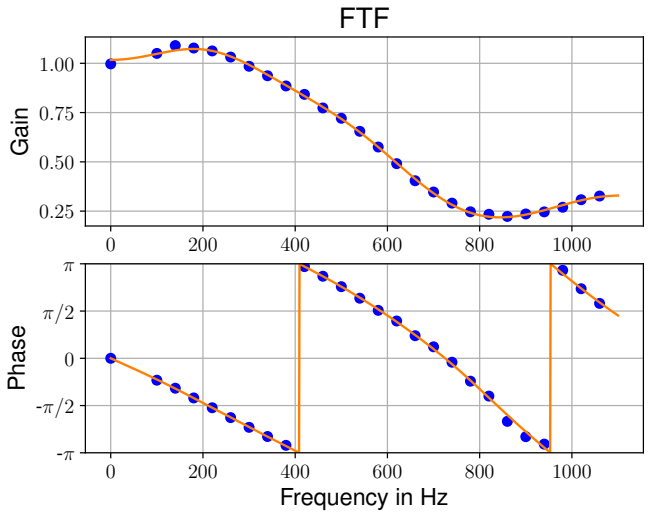

FIGURE 3. Comparison between the state space model approximation of the flame transfer function evaluated at purely real values of ω (orange line) and the data measured from experiments [23] (blue dots).

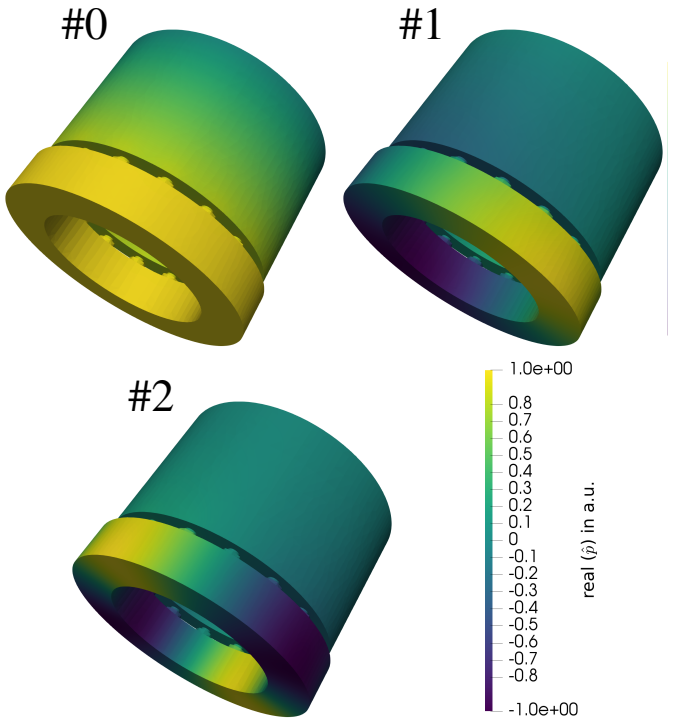

FIGURE 4. Pressure mode shapes of the three thermoacoustic modes considered in this study. They correspond to an axial mode (#0) and plenum-dominant azimuthal modes (#1 and #2).

As explained in the introduction, the perturbation methods proposed in this paper can be also used for uncertainty quantification [8, 9, 10] of the MICCA combustor.

Degeneracy of Thermoacoustic Modes

The analysis focuses on three azimuthal modes with frequencies of 176 Hz, 513 Hz, and 725 Hz, which are mode #0, mode #1 and mode #2, respectively (Fig. 4). Mode #0 is of quarter-wave type in the longitudinal direction. It is stable, featuring a damping rate of $537.9\,\mathrm{s}^{-1}$. The unusually high value damping rate may be attributed to the lack of FTF data far from the real axis. Mode #1 is plenum-dominant and unstable, featuring a growth rate of $366.3\,\mathrm{s}^{-1}$. Mode #2 is also plenum-dominant and marginally-stable, with a growth rate of $0.1\,\mathrm{s}^{-1}$. Because of the degree of rotational symmetry ($N = 16$), a $2\pi/16$ rad rotation of a solution $\widehat{p}$ would also be a valid solution $\widetilde{p}$ to the eigenvalue problem, with the same eigenfrequency. If the azimuthal mode order of $\widehat{p}$ is an integer multiple of $N/2 = 8$, the rotated solution $\widetilde{p}$ and the non-rotated solution $\widehat{p}$ are linearly dependent. This is because if the azimuthal order is an odd multiple of 8, the rotation angle comprises an odd multiple of half of the azimuthal wavelength of the solution. Thus, the rotation establishes the relation $\widetilde{p} = -\widehat{p}$. If the azimuthal order is an even multiple of 8, the rotation angle comprises an even multiple of half of the azimuthal wavelength. Consequently, the relation between the new and the original solution amounts to $\widetilde{p} = \widehat{p}$. If, however, the azimuthal order of the solution is not an integer multiple of 8, the rotated and the original solution are linearly independent. Hence, the rotational symmetry implies that all modes that do not feature an azimuthal mode order being a multiple of 8 are (at least) two-fold degenerate, i.e. there are two linearly independent mode shapes corresponding to the same eigenfrequency. Because there is no other relevant symmetry or special feature present in the model, these modes are expected to have a degeneracy featuring a multiplicity of exactly 2. Indeed, mode #0 is not degenerate while mode #1 and mode #2 are two-fold degenerate.

Perturbation Patterns

As test cases, perturbations of the flame dynamics are considered. These were realized by pre-multiplying the flame transfer functions of the affected burners by the complex-valued scaling factor $(1 + \Delta\varepsilon_n)$, such that gain and phase of the nth flame transfer functions change accordingly. Variations in the magnitude and phase of $\Delta\varepsilon$ affect the gain and phase of the perturbed transfer functions. In this study, the gain of the perturbed flame transfer function is doubled with respect to the baseline configuration. No perturbation of the FTF phase is considered here. This is accomplished by fixing $\Delta\varepsilon_n = \Delta\varepsilon = 1$ at all perturbed burners and $\Delta\varepsilon_n = 0$ at the unperturbed burners, and using the scaling parameter μ as in Eq. (16). For $\mu = 0$ and $\mu = 1$ the baseline and fully-perturbed configurations are obtained, respectively.

Three patterns of perturbed burners along the annulus are studied (Fig. 5). These patterns are chosen because, from the-

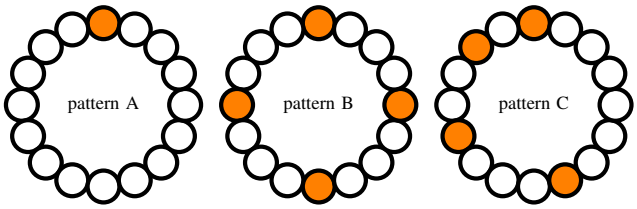

FIGURE 5. Perturbation patterns under consideration. We set $\Delta\varepsilon_n = 1$ at the burners highlighted in orange in these patterns, and $\Delta\varepsilon_n = 0$ at the others.

oretical arguments discussed in more details in the next section together with the results, one expects that

- pattern A breaks the degeneracy of both degenerate modes, leaving one of the resulting eigenmodes unchanged;
- pattern B breaks the degeneracy of mode #2 leaving an eigenmode unchanged, but not that of mode #1;
- pattern C completely breaks the symmetry and the degeneracy is resolved for both modes #1 and #2.

RESULTS

Figure 6 compares the evolution of the eigenfrequencies when predicted with the perturbation approach and computed with a full Helmholtz solver for all considered cases. It can be generally stated that the higher the applied perturbation order, the more accurate the predictions are.

Except for case #1B, the degenerate eigenvalues (modes #1 and #2) split into two. In particular, if a single burner is perturbed, the degenerate eigenvalue (cases #1A and #2A) split into two branches, as expected. In particular, one branch departs from the unperturbed value, but the other does not. This can be explained by considering that, in the two-dimensional degenerate eigenspace, one can always construct a mode shape for which a nodal line exactly crosses the reference point of the perturbed flame transfer function. Therefore, the perturbation has no effect on this mode, and its eigenfrequency does not change. The eigenfrequency associated with the other branch, however, will vary with the perturbation parameter. Qualitatively, this behavior is already correctly predicted by the first-order theory. For the considered perturbation strength, the second-order theory yields quantitatively good results. Only little improvement is obtained by using third-order corrections. Although doubling the gain might be considered a nominally strong perturbation, it actually is not. This is because for this test case only a single burner is perturbed, while the other fifteen remain unchanged. Thus, perturbation theory performs well in this test case.

Also in case #2B one of the degenerate eigenvalues is unaffected by the perturbation, whereas the other is affected. Since mode #2 is of second azimuthal order, there is always a solution in the 2-dimensional eigenspace for which all four perturbed burners of pattern B align with nodal lines. Thus, perturbation pattern B does affect this mode (blue branch). However, for the linearly independent solution (orange branch), there is no such alignment. Hence, the corresponding eigenvalue changes with a change in the perturbation parameter.

In case #1B, since the applied perturbation pattern only reduces the degree of rotational symmetry, the degenerate eigenspace does not unfold. In particular, one can always choose one of the two modes to be aligned with two opposite perturbed burners (left-right), and the other mode to be aligned with the remaining two perturbed burners (top-bottom). Although these two solutions are linearly independent, for symmetry reasons there can be no difference between their eigenvalues – a rotation of 90° maps one onto the other. Therefore, the same change for both branches is expected (and observed) at any order.

Lastly, when the gain of four burners that are arranged in an asymmetric manner is changed – pattern C – the rotational symmetry is completely broken. Therefore, the degenerate eigenspace unfolds into two distinct subspaces (for both mode #1 and #2). We note that, in the non-degenerate scenario, the evolution of the eigenfrequencies of cases #0B and #0C appear to be identical. This is however not true for other perturbation patterns (not shown here). Future work will investigate why perturbation patterns B and C have the same effect on mode #0.

An interesting observation is that the phase (but not the magnitude) of the first-order approximation to the eigenfrequencies only depends on the mode considered, but not on the applied perturbation pattern or the branch considered – ignoring the cases in which the eigenvalue is unaffected by the perturbation, because the slope cannot be uniquely defined for these branches. For example, the first-order slope of the orange branch of case #1A is the same as that of all branches in #1B and #1C. This can be formally explained by exploiting both the rotational and the reflection symmetries of the model set-up, and is the topic of the next section.

INCLINATION OF FIRST-ORDER SENSITIVITY

The test cases have shown that, if the same perturbation is applied to an arbitrary number of burners, the first-order theory predicts the change in eigenfrequencies to have the same slope, regardless of how many burners are perturbed. More precisely, if one specific mode is considered, the phase angle of the first-order eigenfrequency correction $\angle\omega_1$ is a function of the perturbation of the FTF only. This section shortly outlines a proof, showing that the reason for this is the reflection symmetry of the unperturbed MICCA model.

Because of the rotational symmetry of the unperturbed MICCA model, the corresponding eigenfunctions can be repre-

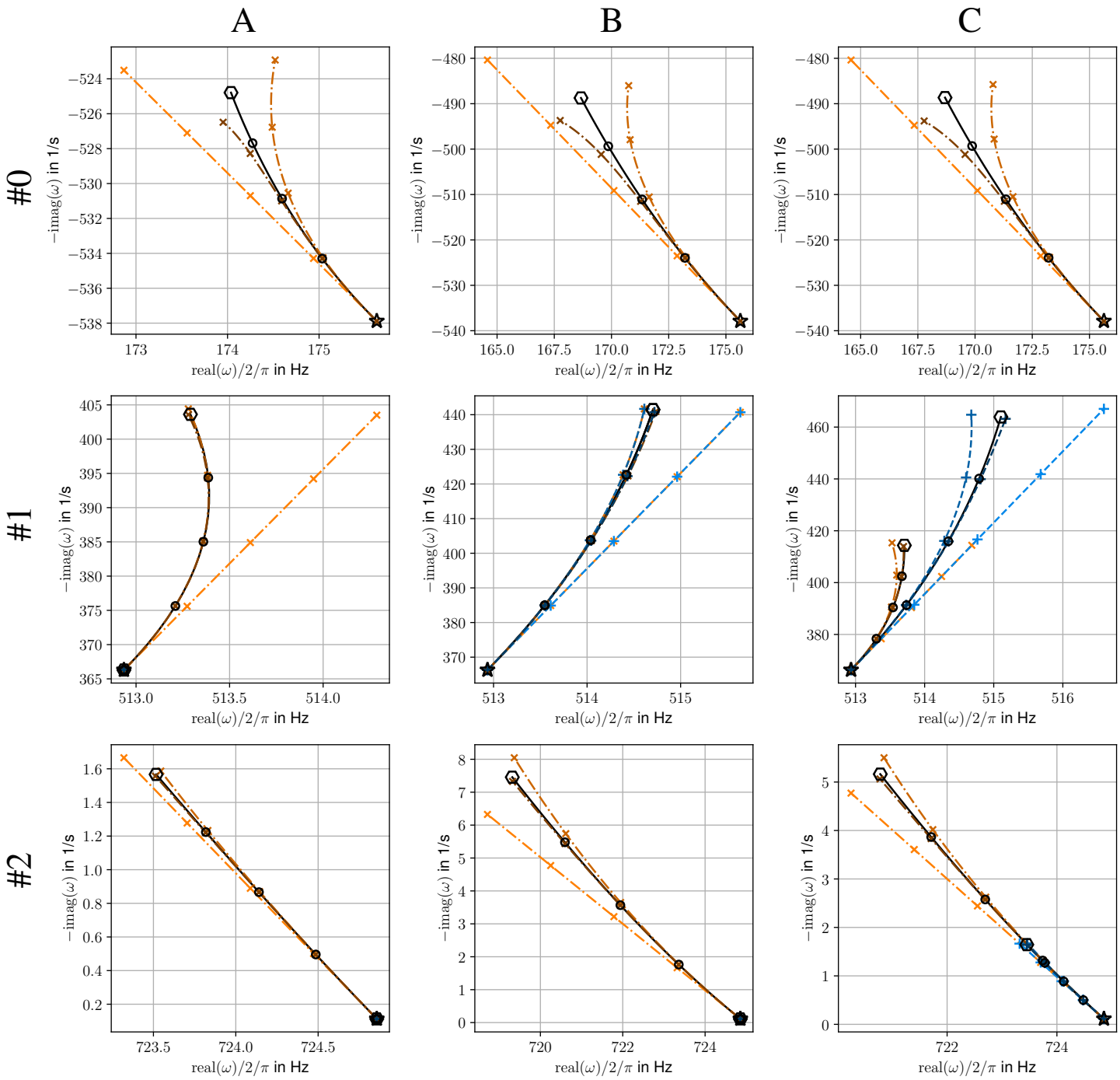

FIGURE 6. Eigenvalue evolution of various modes (rows) for different perturbation patterns (columns). The black curves with markers denote the exact results for perturbation parameters μ of 0.00 (☆), 0.25 (○), 0.50 (○), 0.75 (○), and 1.00 (○). The degenerate eigenvalues might split into two branches – orange line with (x)-markers and blue line with (+)-markers. The darker the shading, the higher the applied order of the perturbation theory. Note, that for the cases #1A, #2A and #2B, an eigenvalue is unaffected by the perturbations, and therefore it reduces to a single (blue) point.

sented as Bloch-waves [27], i.e., functions of the following form:

$$\widehat{p} = \exp(\mathrm{i}b\varphi)\psi_b(\varphi) \tag{21}$$

Here, b is the Bloch-wavenumber and $\psi_b(\varphi)$ is a function periodic in the angular coordinate with periodicity $\psi_b(\varphi) = \psi_b(\varphi + \frac{2\pi}{N})$, where N denotes the degree of rotational symmetry of the considered, unperturbed system. If the system features an additional reflection symmetry, as it is the case for the MICCA, then it can be shown that the two Bloch-waves corresponding to the Bloch-wave numbers $+b$ and $-b$ feature the same eigenfrequency – see [11] for an introduction into Bloch-wave theory with focus on thermoacoustic systems.

It can be seen that a scalar multiple of a Bloch-wave is also a Bloch-wave with the same Bloch-wave number b. Furthermore, the angular derivative reads

$$\partial_\varphi \exp(\mathrm{i}b\varphi)\psi_b(\varphi) = \mathrm{i}b\exp(\mathrm{i}b\varphi)\psi_b(\varphi) + \exp(\mathrm{i}b\varphi)\partial_\varphi\psi_b(\varphi) \tag{22}$$

$$= \exp(\mathrm{i}b)\underbrace{\left[\mathrm{i}b\psi_b(\varphi) + \partial_\varphi\psi_b(\varphi)\right]}_{\widetilde{\psi}_b(\varphi)}. \tag{23}$$

Because the function $\widetilde{\psi}_b(\varphi)$ is also periodic with period $\frac{2\pi}{N}$, the angular derivative is still a Bloch wave with Bloch-wavenumber b. As the linear operator $\mathcal{L}_{0,0}$ and all its derivatives $\mathcal{L}_{m,0}$ are linear combinations of scalar-multiplications and rotationally symmetric spatial derivatives, the product $\mathcal{L}_{m,0}\widehat{p}$ is a Bloch wave of Bloch-wavenumber b if $\widehat{p}$ is Bloch wave of Bloch-wavenumber b.

It can be easily shown that Bloch waves featuring different Bloch-wavenumbers are pairwise orthogonal. Thus, for a degenerate mode, the appropriate Bloch waves of Bloch-wavenumber $+b$ and $-b$ can be chosen as bases for the direct and the adjoint eigenspace, $\{\widehat{p}_b, \widehat{p}_{-b}\}$ and $\{\widehat{p}^\dagger_b, \widehat{p}^\dagger_{-b}\}$ say. They are already bi-orthogonal with respect to the inner product $\left\langle \widehat{p}^\dagger_i \middle| \mathcal{L}_{1,0}\widehat{p}_j \right\rangle$. Hence, they can be scaled such that the auxiliary matrix $\boldsymbol{Y}$ in Eq. (13) equals the identity matrix and the deployed bases are of Bloch-wave type. With this choice of basis-functions, the diagonal elements of the first-order auxiliary matrix $\boldsymbol{X}_1$ are

$$\left\langle \widehat{p}^\dagger_{\pm b} \middle| \mathcal{L}_{0,1}\widehat{p}_{\pm b} \right\rangle = \sum_{n=0}^{N-1} \left\langle \widehat{p}^\dagger_{\pm b} \middle| \mathcal{L}_{0,1}\widehat{p}_{\pm b} \right\rangle_n, \tag{24}$$

where the notation $\langle\cdot|\cdot\rangle_n$ denotes the contribution to the scalar product $\langle\cdot|\cdot\rangle$ from the sector covering an angle from $(n-\frac{1}{2})\frac{2\pi}{N}$ to $(n+\frac{1}{2})\frac{2\pi}{N}$ – a so-called unit cell. Analogously,

$$\left\langle \widehat{p}^\dagger_{\mp b} \middle| \mathcal{L}_{0,1}\widehat{p}_{\pm b} \right\rangle = \sum_{n=0}^{N-1} \left\langle \widehat{p}^\dagger_{\mp b} \middle| \mathcal{L}_{0,1}\widehat{p}_{\pm b} \right\rangle_n \tag{25}$$

is found for the off-diagonal elements.

For a single perturbation parameter, i.e., when the *same* perturbation $\Delta\varepsilon$ is applied to any number of burners, the operator derivative in sector n is either $\mathcal{L}_{0,1} = -\frac{\gamma-1}{\rho_0}\mathrm{FTF}(\omega)\nabla(\cdot)_{\mathrm{ref}}\cdot\vec{n}_{\mathrm{ref}}$ (identical in all perturbed burners) or $\mathcal{L}_{0,1} = 0$, depending on whether the unit cell contains a perturbed burner or not. Consequently, only sectors containing a perturbed burner contribute to the scalar products. Moreover, because of the point support of the flame response, only a single point of each of these sectors is actually relevant. The Bloch waves featuring Bloch-wavenumber of opposite sign can be converted into each other by reflection across a symmetry line. This symmetry line can be chosen to cross the reference point in sector 0 so that the values of the direct eigensolutions at this point are identical. The same is true for the adjoint solutions. Due to Bloch-periodicity the values at the reference points in the other sectors can then be expressed as $\widehat{p}(0)\exp(-\mathrm{i}[\pm b]n\frac{2\pi}{N})$ and $\widehat{p}^\dagger(0)\exp(-\mathrm{i}[\pm b]n\frac{2\pi}{N})$. Plugging this relation into the definition of the auxiliary matrix $\boldsymbol{X}_1$ – Eq. (13) – yields

$$\boldsymbol{X}_1 = \left\langle \widehat{p}^\dagger(0) \middle| \mathcal{L}_{0,1}\widehat{p}(0) \right\rangle_0 \underbrace{\sum_{n\in\mathrm{per.}} \begin{bmatrix} 1 & \exp(\mathrm{i}2bn\frac{2\pi}{N}) \\ \exp(-\mathrm{i}2bn\frac{2\pi}{N}) & 1 \end{bmatrix}}_{\boldsymbol{\chi}} \tag{26}$$

Because the matrix $\boldsymbol{\chi}$ is Hermitian, its eigenvalues are real. Thus, regardless the number of the perturbed burners, the phase of $\Delta\varepsilon\left\langle \widehat{p}^\dagger(0) \middle| \mathcal{L}_{0,1}\widehat{p}(0) \right\rangle_0$ is the same as that of the eigenvalues of $\boldsymbol{X}_1$, modulo phase shift of π if the eigenvalues of $\boldsymbol{\chi}$ are negative. Note that $\boldsymbol{\chi}$ depends on the distribution pattern of the perturbed burners only, and it can argued that the Bloch-wavenumber b is equivalent to the azimuthal mode order. Hence, $\sum_{n\in\mathrm{per.}}\exp(\mathrm{i}2bn\frac{2\pi}{N})$ is the second coefficient of the Fourier transform of the burner arrangement pattern. Thus, the above first-order splitting theory has analogies with the so called C_{2n}-criterion presented in [14].

The above rationale can be generalized to predict the first-order eigenvalue drift for different perturbations of the burners. An interesting case is obtained when two separate sets of burners are perturbed in different ways such that the FTF perturbations have the same phase and average to zero. For these perturbations, it can be proven that the eigenvalue splits in opposite directions. We demonstrate this numerically without a formal proof in this paper; a detailed discussion of this generalized theory is beyond the scope of the present contribution and left for future work. We consider perturbation pattern C applied to mode #1; additionally, to compensate for the change in the total FTF gain due to its local increase in the burners of pattern C, the gain of the other 12 is reduced at these burners, so that the average FTF gain variation vanishes. For example, when $\Delta\varepsilon_1 = 1$ at the 4 burners highlighted in pattern C, then $\Delta\varepsilon_2 = -1/3$ at the other 12 burners, so that, on average, $\Delta\varepsilon = 0$.

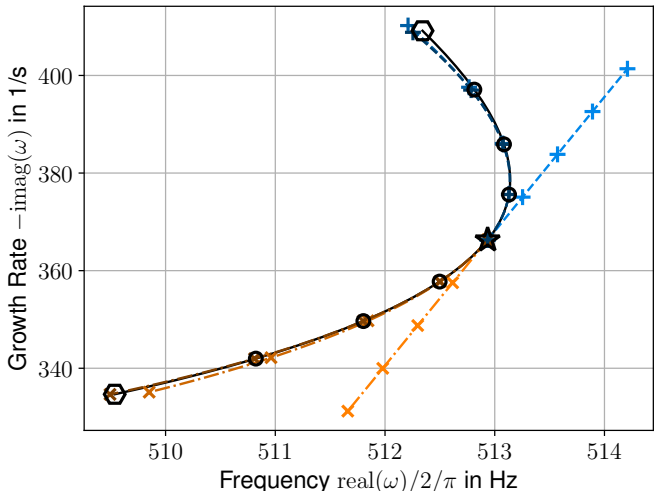

FIGURE 7. Eigenvalues evolution for mode #1 when a modified version of pattern C is applied such that the average change to the FTFs is 0. As expected, the first-order theory predicts a shift of the eigenvalues in opposite directions.

The variation of the eigenvalues for increasing values of the perturbation parameters is shown in Fig. 7. Despite the variation of the eigenvalues being nonlinear, the first-order theory predicts the two degenerate eigenvalues to split precisely in opposite directions. It is therefore impossible to make a certain combustor more stable by applying this type of perturbation: if the growth rate of one of the split eigenvalues is decreased, as a consequence, that of the other one is increased. This complements the findings of [28], in which it was shown that, in a weakly coupled, linear limit, the most stable configuration in a combustor in which two types of flames can be arbitrarily distributed is one that consists of a single type of flames. Whether this remains true at higher orders or in a non-weak coupling limit could be addressed with an extension of the theory outlined above.

CONCLUSIONS

First, second, and third order adjoint perturbation theory was successfully used to predict the eigenfrequency evolution of thermoacoustic modes in a practical three-dimensional combustor model. In particular, a possible split of the degenerate modes into two non-degenerate solutions due to the loss of rotational symmetry can be accurately predicted with this theory. The findings are useful for the fast assessment of the thermoacoustic stability of multiple combustor variants derived from the same rotationally symmetric baseline configuration. For the presented model it takes about 24 s to solve the nonlinear eigenvalue problem for one set of parameters with the current implementation of PyHoltz. On the contrary, it just takes approximately 5 s to compute the polynomial coefficients for the power series approximation with perturbation theory from one such solution. Even though it was not done in this study, as the baseline configuration features a discrete rotational symmetry, its solution can be further accelerated via unit-cell computations facilitated by Bloch-wave theory. Moreover, the theory is not limited to Helmholtz-based models because it is a general technique for the approximative solution of nonlinear eigenvalue problems. The adjoint-perturbation approach and the effects of asymmetry, thus, analogously apply to network models and models based on linearized Euler equations. The adjoint perturbation theory can also improve numerical methods for finding solutions of the nonlinear eigenvalue problem associated with thermoacoustic stability assessment. For example, in the current study, the iterative solver for the nonlinear eigenvalue problem has been initialized with the predictions from perturbation theory to find the two branches into which a degenerate solution splits due to symmetry-breaking, an otherwise complicated task as the two branches lie closely together.

Moreover, it was proven that the eigenfrequency of a mode departs with the same inclination – the phase in the complex plane – from the expansion point in the complex plane if the perturbed burners are modified in the same manner, regardless of how many burners are perturbed. The inclination rule can practically guide the design process of new gas turbines, and the benefits of adjoint perturbation theory significantly improve the speed at which a family of annular and can-annular combustor designs can be assessed. For both reasons the findings of this study can contribute to the improvement of the industrial design process of new gas turbines.

ACKNOWLEDGMENT

We are grateful to Davide Laera for providing the modeling data of the MICCA combustor. We also thank Philip E. Buschmann for his help with the implementation of the python code. Alessandro Orchini is grateful to the Alexander von Humboldt Foundation for financial support through the Humboldt Research Fellowship for Postdoctoral Researchers. Luca Magri gratefully acknowledges the support from the Royal Academy of Engineering Research Fellowships Scheme.

REFERENCES

[1] Lieuwen, T., 2005. "Nonlinear kinematic response of premixed flames to harmonic velocity disturbances". *Proc. Combust. Inst.,* ***30***(2), pp. 1725–1732.

[2] Dowling, A. P., and Mahmoudi, Y., 2015. "Combustion noise". *Proceedings of the Combustion Institute,* ***35***(1), pp. 65–100.

[3] Poinsot, T., 2017. "Prediction and control of combustion instabilities in real engines". *Proc. Combust. Inst.,* ***36***(1), pp. 1–28.

[4] Dowling, A. P., 1995. "The calculation of thermoacoustic oscillations". *J. Sound Vib.,* ***180***(4), pp. 557–581.

[5] Nicoud, F., Benoit, L., Sensiau, C., and Poinsot, T., 2007. "Acoustic modes in combustors with complex impedances and multidimensional active flames". *AIAA Journal,* ***45***(2), pp. 426–441.

[6] Magri, L., and Juniper, M. P., 2013. "Sensitivity analysis of a time-delayed thermo-acoustic system via an adjoint-based approach". *J. Fluid Mech.,* ***719***(2013), pp. 183–202.

[7] Orchini, A., and Juniper, M. P., 2015. "Linear stability and adjoint sensitivity analysis of thermoacoustic networks with premixed flames". *Combust. Flame,* ***165***, pp. 97–108.

[8] Magri, L., Bauerheim, M., Nicoud, F., and Juniper, M. P., 2016. "Stability analysis of thermo-acoustic nonlinear eigenproblems in annular combustors. Part II. Uncertainty quantification". *J. Comput. Phys.,* ***325***, pp. 411–421.

[9] Silva, C. F., Magri, L., Runte, T., and Polifke, W., 2016. "Uncertainty Quantification of Growth Rates of Thermoacoustic Instability by an Adjoint Helmholtz Solver". *J. Eng. Gas Turbines Power,* ***139***(1), p. 011901.

[10] Mensah, G. A., Magri, L., and Moeck, J. P., 2018. "Methods for the calculation of thermoacoustic stability boundaries and monte carlo-free uncertainty quantification". *J. Eng. Gas Turbines Power,* ***140***(6), p. 061501.

[11] Mensah, G. A., and Moeck, J. P., 2015. "Efficient computation of thermoacoustic modes in annular combustion chambers based on Bloch-wave theory". In ASME Turbo Expo, pp. GT2015–43476.

[12] Mensah, G. A., and Moeck, J. P., 2017. "Acoustic Damper Placement and Tuning for Annular Combustors: An Adjoint-Based Optimization Study". *J. Eng. Gas Turbines Power,* ***139***(6), p. 061501.

[13] Moeck, J. P., Paul, M., and Paschereit, C. O., 2010. "Thermoacoustic Instabilities in an Annular Rijke Tube". *Proc. ASME Turbo Expo 2010*, pp. 1219–1232.

[14] Noiray, N., Bothien, M., and Schuermans, B., 2011. "Investigation of azimuthal staging concepts in annular gas turbines". *Combustion Theory and Modelling,* ***15***(5), pp. 585–606.

[15] Parmentier, J.-F., Salas, P., Wolf, P., Staffelbach, G., Nicoud, F., and Poinsot, T., 2012. "A simple analytical model to study and control azimuthal instabilities in annular combustion chambers". *Combustion and Flame,* ***159***(7), pp. 2374–2387.

[16] Bauerheim, M., Ndiaye, A., Constantine, P., Moreau, S., and Nicoud, F., 2016. "Symmetry breaking of azimuthal thermoacoustic modes: the UQ perspective". *J. Fluid Mech.,* ***789***, pp. 534–566.

[17] Lancaster, P., 1961. "A generalised Rayleigh quotient iteration for lambda-matrices". *Arch. Rational Mech Anal.,* ***8***, pp. 309–322.

[18] Güttel, S., and Tisseur, F., 2017. "The nonlinear eigenvalue problem". *Acta Numerica,* ***26***, May, pp. 1–94.

[19] Magri, L., Bauerheim, M., and Juniper, M. P., 2016. "Stability analysis of thermo-acoustic nonlinear eigenproblems in annular combustors. Part I. Sensitivity". *J. Comput. Phys.,* ***325***, pp. 395–410.

[20] Bourgouin, J.-F., Durox, D., Moeck, J., Schuller, T., and Candel, S., 2014. "Characterization and modeling of a spinning thermoacoustic instability in an annular combustor equipped with multiple matrix injectors". *Journal of Engineering for Gas Turbines and Power,* ***137***, p. 021503 (11 pages).

[21] Bourgouin, J.-F., Durox, D., Moeck, J., Schuller, T., and Candel, S., 2014. "A new pattern of instability observed in an annular combustor: the slanted mode". *Proceedings of the Combustion Institute,* ***35***, pp. 3237–3244.

[22] Prieur, K., Durox, D., and Schuller, T., 2017. "A hysteresis phenomenon leading to spinning or standing azimuthal instabilities in an annular combustor". *Combustion and flame,* ***175***, pp. 283–291.

[23] Laera, D., Schuller, T., Prieur, K., Durox, D., Camporeale, S. M., and Candel, S., 2017. "Flame describing function analysis of spinning and standing modes in an annular combustor and comparison with experiments". *Combustion and Flame,* ***184***, pp. 136 – 152.

[24] Mensah, G. A., and Moeck, J. P., 2017. "Limit cycles of spinning thermoacoustic modes in annular combustors: A bloch-wave and adjoint-perturbation approach". *ASME Paper GT2017-64817*.

[25] Gustavsen, B., and Semlyen, A., 1999. "Rational approximation of frequency domain responses by vector flltlng". *IEEE Transactions on Power Delivery,* ***14***(3), July, pp. 1052–1061.

[26] Gustavsen, B., 2006. "Improving the pole relocating properties of vector fitting". *IEEE Transactions on Power Delivery*.

[27] Bloch, F., 1929. "Über die Quantenmechanik der Elektronen in Kristallgittern". *Zeitschrift für Physik,* ***52***, pp. 555–560.

[28] Bauerheim, M., Salas, P., Nicoud, F., and Poinsot, T., 2014. "Symmetry breaking of azimuthal thermo-acoustic modes in annular cavities: a theoretical study". *Journal of Fluid Mechanics,* ***760***, pp. 431–465.